LETTERS

Ultrasensitive solution-cast quantum dot photodetectors

Gerasimos Konstantatos[1], Ian Howard[1], Armin Fischer[1], Sjoerd Hoogland[1], Jason Clifford[1], Ethan Klem[1], Larissa Levina[1] & Edward H. Sargent[1]

Solution-processed electronic[1] and optoelectronic[2–5] devices offer low cost, large device area, physical flexibility and convenient materials integration compared to conventional epitaxially grown, lattice-matched, crystalline semiconductor devices. Although the electronic or optoelectronic performance of these solution-processed devices is typically inferior to that of those fabricated by conventional routes, this can be tolerated for some applications in view of the other benefits. Here we report the fabrication of solution-processed infrared photodetectors that are superior in their normalized detectivity ($D^\star$, the figure of merit for detector sensitivity) to the best epitaxially grown devices operating at room temperature. We produced the devices in a single solution-processing step, overcoating a prefabricated planar electrode array with an unpatterned layer of PbS colloidal quantum dot nanocrystals. The devices showed large photoconductive gains with responsivities greater than $10^3\,\mathrm{A\,W^{-1}}$. The best devices exhibited a normalized detectivity $D^\star$ of 1.8×10^{13} jones (1 jones = $1\,\mathrm{cm\,Hz^{1/2}\,W^{-1}}$) at $1.3\,\mu\mathrm{m}$ at room temperature: today's highest performance infrared photodetectors are photovoltaic devices made from epitaxially grown InGaAs that exhibit peak $D^\star$ in the 10^{12} jones range at room temperature, whereas the previous record for $D^\star$ from a photoconductive detector lies at 10^{11} jones. The tailored selection of absorption onset energy through the quantum size effect, combined with deliberate engineering of the sequence of nanoparticle fusing and surface trap functionalization, underlie the superior performance achieved in this readily fabricated family of devices.

Sensing beyond $1\,\mu\mathrm{m}$ into the short-wavelength infrared is critical to environmental monitoring and remote sensing[6–9], fibre-optic communications, night-time surveillance[10] and emerging medical imaging modalities[11–13]. The photosensitive properties of silicon deteriorate rapidly beyond 800 nm and end abruptly at $1.1\,\mu\mathrm{m}$. It is therefore of great interest to produce infrared photodetectors via facile processing from solution, thereby enabling convenient monolithic integration with silicon integrated circuits.

Infrared photodetector sensitivity is quantified using the parameter $D^\star$, the normalized detectivity measured in units of jones (cm $\mathrm{Hz^{1/2}\,W^{-1}}$). $D^\star$ is given as $(A\Delta f)^{1/2}R/i_n$, where A is the effective area of the detector in $\mathrm{cm^2}$, Δf the electrical bandwidth in Hz, and R the responsivity in $\mathrm{A\,W^{-1}}$ measured under the same conditions as the noise current i_n in A. The material figure of merit $D^\star$ allows comparison among devices of different areas and geometries. The device figure of merit, noise equivalent power (NEP)—the minimum impinging optical power that a detector can distinguish from noise—is related to $D^\star$ by NEP = $(A\Delta f)^{1/2}/D^\star$.
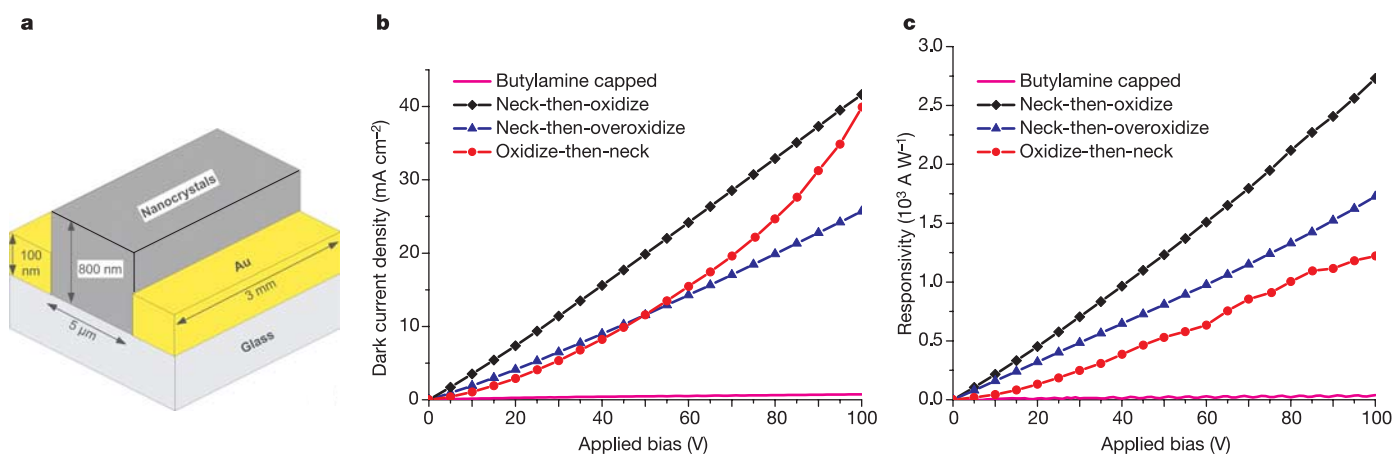
Figure 1 | Device structure and electro-optic characteristics for device classes investigated. a, Device structure. Smooth films of controlled thickness were formed by spin-coating nanocrystals from chloroform solution. **b**, Dark current density. Nanocrystal necking by way of soaking in methanol resulted in two orders of magnitude increase in dark current density. Devices made using nanocrystals exposed to oxygen before film formation ('oxidize-then-neck') show a superlinear I–V behaviour characteristic of field-assisted transport. Devices made using nanocrystals necked before oxidization exhibit linear (field-independent) behaviour. Further oxidation of neck-then-oxidize devices (neck-then-overoxidize) leads to a decrease of conductivity owing to excessive oxide formation. **c**, Responsivity as a function of applied bias. Necked nanocrystal devices show comparable responsivities, consistent with similar carrier mobilities and trap state lifetimes.

[1]Department of Electrical and Computer Engineering, University of Toronto, 10 King's College Road, Toronto, Ontario M5S 3G4 Canada.

The thermodynamic upper bound on D^* is fundamentally determined by the bandgap of the semiconductor used as the light-absorbing medium. Smaller-bandgap materials absorb more low-energy thermal photons, increasing noise. The ideal medium for photodetection would therefore be one that is spectrally tunable, tailored optimally to use the largest effective bandgap that nevertheless absorbs all photons of interest in a particular application. Practical limits on experimentally achieved D^* values are explained in terms of excess noise. Polycrystalline photoconductive detectors[14], for example, exhibit multiplicative noise[15] associated with the product of transport noise with fundamental generation-recombination noise in band-edge and trap states.

Colloidal semiconductor quantum dots offer a simultaneous solution to the aforementioned challenges: they are processed from solution, allowing convenient integration with any substrate; they can be tuned by way of the quantum size effect[16], allowing the effective bandgap to be selected optimally for a given application;
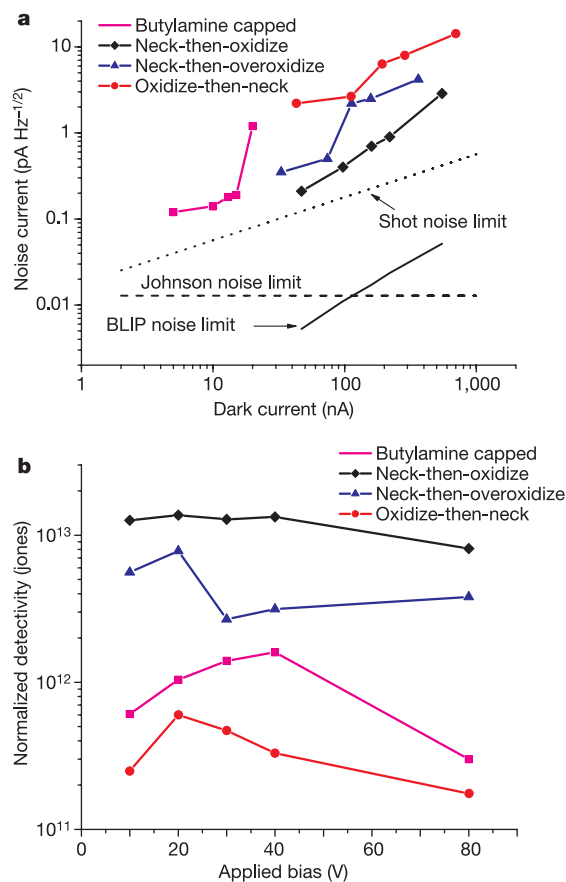
Figure 2 | Noise characteristics and resultant normalized detectivity of the different device classes investigated. a, Measured noise current as a function of measured dark current. Neck-then-oxidize devices exhibited the lowest noise current that approaches within 3 dB the shot noise limit. Oxidize-then-neck nanocrystal devices had the highest noise current consistent with multiplicative noise. Devices formed from neck-then-overoxidize nanocrystals showed lower noise levels than the oxidize-then-neck nanocrystal devices although they contained larger amounts of oxide. This indicates the criticality of the oxidation step in the fabrication process. The Johnson noise limit, the shot-noise limit, and fundamental background-limited thermodynamic (BLIP) noise current of the best-performing devices (neck-then-oxidize) are also plotted for comparison. **b,** Normalized detectivity D^* as a function of applied bias. Oxidize-then-neck devices demonstrated the lowest detectivity. The highest detectivity was obtained from neck-then-oxidize devices measured at a modulation frequency of 30 Hz, and reached 1.3×10^{13} jones at 975 nm excitation wavelength.

and their transport and trap state properties can be separately controlled through the engineering of ligands and the oxidation of nanoparticle surfaces either before or after film formation. Cross-linking of semiconductor nanoparticles has previously been shown to result in marked increases in film conductivity[17,18]. In addition, visible photoconduction has been reported in pure CdSe nanocrystal films following chemical treatment[19–21]. However, there exists only one previous observation of infrared photoconductivity[5], and there have been no previous reports of quantified photodetector sensitivity from such materials.

We fabricated photoconductive detectors by spin-coating colloidal quantum dots from solution onto gold interdigitated electrodes. The inter-electrode separation was $5\,\mu m$ and the metal electrode height was 100 nm. The resultant structure is depicted in Fig. 1a. The thickness of the quantum dot films formed was 800 nm.

Devices synthesized using PbS nanocrystals capped with oleic acid[22] were found to be insulating. The $\sim$2.5-nm-long ligand inhibited carrier transport among the nanocrystals. To improve carrier mobility, we used a post-synthetic ligand exchange to replace oleic acid with n-butylamine of length $\sim$0.6 nm. Ligand exchange, confirmed via Fourier transform infrared spectroscopy (FTIR; Supplementary Information 1), resulted in decreased interparticle spacing as observed via transmission electron microscopy (TEM; Supplementary Information 1). The conductance after exchange was low but measurable, producing a dark current density of $\sim$0.7 mA cm^{-2} at 100 V bias. We therefore immersed devices in methanol (MeOH) for 2 hours to remove butylamine ligands and further decrease interparticle separation, causing necking, or cross-linking, at points where adjacent nanoparticles' surfaces are in contact with one another (Supplementary Information 2). The dark current density increased by two orders of magnitude to $\sim$40 mA cm^{-2}.
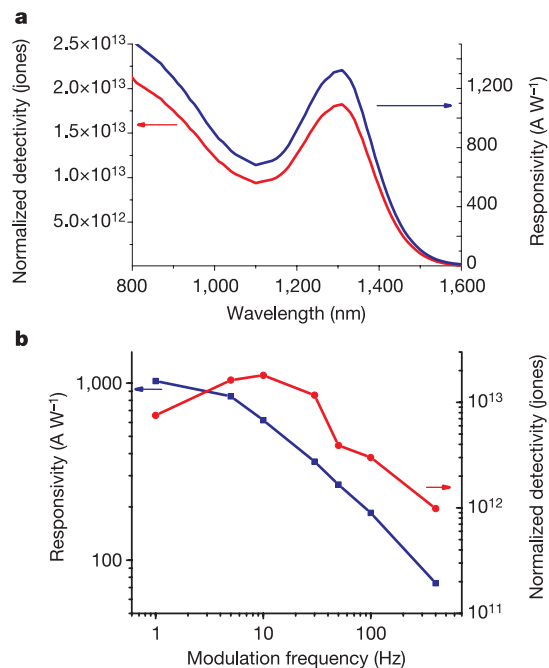
Figure 3 | Photodetector performance characteristics of the highest-sensitivity class of devices. a, Spectra of responsivity and normalized detectivity D^* of neck-then-oxidize nanocrystal devices. The applied bias is 40 V and the electrical frequency 10 Hz. D^* was measured to be 1.8×10^{13} jones at the excitonic peak wavelength. **b,** Electrical frequency response of the same devices under 40 V bias. The 3-dB bandwidth of the detectors is $\sim$18 Hz, consistent with the longest excited-state carrier lifetime in these devices. High sensitivity ($D^* > 10^{13}$ jones) is retained at imaging rates of 30 frames per second.

Photoconductivity relies on long-lived trap states to enable photo-conductive gain. However, to suppress the multiplicative noise to which conventional polycrystalline photoconductive detectors are prone, it is necessary to minimize transport noise associated with trap states lying at the interface between quantum dots. We therefore fabricated two classes of devices, one intended to minimize multiplicative noise, the other to serve as control. In devices labelled 'neck-then-oxidize', we maintained oxygen-free conditions throughout all process steps before film fabrication, sensitizing by means of oxidation only at the end. In devices labelled 'oxidize-then-neck', we precipitated the colloidal quantum dots from their butylamine solvent in oxygen-rich ambient conditions.

X-ray photoelectron spectroscopy (XPS; Supplementary Information 3) showed that butylamine-capped nanocrystals precipitated in inert conditions were free from $PbSO_4$, the trap-state-forming oxide native to PbS. Butylamine-capped nanocrystals precipitated in inert conditions and then treated by methanol soaking (neck-then-oxidize) consisted predominantly of PbS, but exhibited a measurable $PbSO_4$ level estimated at 5% (that is, 5% of Pb atoms were bound to sulphate groups instead of sulphur). Butylamine-capped nanocrystals precipitated in an air ambient (oxidize-then-neck) exhibited a significant amount of $PbSO_4$ formation, with a sulphate fraction now at 25%. These observations regarding sulphate levels were confirmed using FTIR (Supplementary Information 3).

As shown in Fig. 1b, the order of operations in necking versus oxidizing does not significantly influence the magnitude of the dark current. However, it does influence the shape of the dark current versus voltage (I–V) characteristic. Neck-then-oxidize devices exhibit a linear (field-independent) I–V characteristic, suggesting that nanocrystal necking was achieved and the dominant conduction mechanism was variable range hopping[23]. Oxidize-then-neck devices exhibited a superlinear (higher slope at higher biases) I–V characteristic, suggesting that transport in these devices is field-assisted owing to sulphate barriers formed along the pathway of carrier transport.

The signal component of the sensitivity of photodetectors is quantified by the responsivity. Figure 1c shows the measured responsivity as a function of the applied bias for devices excited using a 975-nm laser. The optical power impinging on each device was ~80 pW (Supplementary Information 4). Responsivity correlated closely with dark current, indicating that high responsivities were associated with the successful removal of ligands that led to nanocrystal necking. Long trap state lifetimes, also necessary for photoconductive gain, were amply achieved in all devices with the aid of oxidation of the high-surface-to-volume nanometre-sized semiconductor particles.

We investigated experimentally the transit time and the longest tail of carrier lifetime to provide independent confirmation of the existence of such strikingly high photoconductive gain. The response of the detector to a 7-ns optical pulse was found to persist over tens of milliseconds, attributable to the longest-lived population of trap states introduced by oxidation[24] (Supplementary Information 5). The response exhibits multiple lifetime components that extend from microseconds to several milliseconds (decay components were found at ~20 µs, ~200 µs, 2 ms, 7 ms and 70 ms). We obtained transit times of 500 ns at a bias of 100 V (ref. 25), finding that transit time depended linearly on bias with a slope corresponding to a mobility of $0.1\ cm^2\ V^{-1}\ s^{-1}$, consistent with prior reports[1]. The ratio of the longest component of carrier lifetime to the transit time was thus of the order of 10,000. Our observed responsivities of $2,700\ A\ W^{-1}$ are thus explainable by photoconductive gain, given our films' absorbance of 0.3 at an optical wavelength of 975 nm. We note also that this high responsivity was observed under the low-level optical power conditions relevant to ultrasensitive detection. As we increased illumination intensity, the longest-lived trap states became filled, and shorter-lived, hence lower-gain trap states began to account for a significant component of carrier lifetime. The devices

were thus most sensitive under low-light illumination conditions, and exhibit intrinsic dynamic-range-enhancing gain compression under increasing illumination.

Achieving sensitive detection requires not only high responsivity, but also low noise. We plot in Fig. 2a the measured noise current versus the dark current for each class of devices. Neck-then-oxidize nanoparticles approach the shot noise limit within 3 dB. Oxidize-then-neck devices lie at least 15 dB from fundamental noise limits. We measured the noise current and, combining this with the responsivity, obtained the normalized detectivity D^* (Supplementary Information 6). Figure 2b shows D^* of the photodetectors at different bias conditions, measured at an optical excitation wavelength of 975 nm and a modulation frequency of 30 Hz. The most sensitive devices were those labelled neck-then-oxidize, from which $D^* > 10^{13}$ jones was obtained.

The electro-optic characteristics of a typical ultrasensitive detector are presented in Fig. 3 (Supplementary Information 7). Figure 3a shows the spectral responsivity and normalized detectivity for electrical modulation frequency 30 Hz and applied bias 40 V. The responsivity spectrum corresponds closely to the absorption spectrum. Figure 3b presents the frequency response of the detector under modulated illumination. The 3-dB bandwidth is ~18 Hz, consistent with the longest carrier lifetime component at 70 ms. D^* remains in excess of 10^{13} jones at the 30 frames-per-second required for imaging.

Reproducibility of all results reported here was confirmed by fabricating several devices using nanocrystals from several different synthesis batches. Preliminary studies of device lifetime indicate that the performance of devices stored in air for 2 weeks does not change by more than 20%; and that devices stored in a nitrogen glovebox do not, over the course of months, change more than 20% in performance.

1. Talapin, D. & Murray, C. B. PbSe nanocrystal solids for n- and p-channel thin film field-effect transistors. *Science* 310, 86–89 (2005).
2. Tessler, N., Medvedev, V., Kazes, M., Kan, S. & Banin, U. Efficient near-infrared polymer nanocrystal light-emitting diodes. *Science* 295, 1506–1508 (2002).
3. Konstantatos, G., Huang, C., Levina, L., Lu, Z. & Sargent, E. H. Efficient infrared electroluminescent devices using solution-processed colloidal quantum dots. *Adv. Funct. Mater.* 15, 1865–1869 (2005).
4. Hoogland, S. *et al.* A solution-processed 1.53 µm quantum dot laser with temperature-invariant emission wavelength. *Opt. Express* 14, 3273–3281 (2006).
5. McDonald, S. A. *et al.* Solution-processed PbS quantum dot infrared photodetectors and photovoltaics. *Nature Mater.* 4, 138–142 (2005).
6. Schödel, R. *et al.* A star in a 15.2-year orbit around the supermassive black hole at the centre of the Milky Way. *Nature* 419, 694–696 (2002).
7. Rawlings, S. *et al.* A radio galaxy at redshift 4.41. *Nature* 383, 502–505 (1996).
8. Ettl, R., Chao, I., Diederich, F. & Whetten, R. L. Isolation of C_{76}, a chiral (D_2) allotrope of carbon. *Nature* 353, 149–153 (1991).
9. Walker, J. Tunable alkali halide lasers. *Nature* 256, 695 (1975).
10. Ettenberg, M. A little night vision. *Adv. Imaging* 20, 29–32 (2005).
11. Sargent, E. H. Infrared quantum dots. *Adv. Mater.* 17, 515–522 (2005).
12. Lim1, Y. T. *et al.* Selection of quantum dot wavelengths for biomedical assays and imaging. *Mol. Imaging* 2, 50–64 (2003).
13. Kim, S. *et al.* Near-infrared fluorescent type II quantum dots for sentinel lymph node mapping. *Nature Biotechnol.* 22, 93–97 (2004).
14. Petritz, R. L. Theory of photoconductivity in semiconductor films. *Phys. Rev. B* 104, 1508–1516 (1956).
15. Carbone, A. & Mazzetti, P. Grain-boundary effects on photocurrent fluctuations in polycrystalline photoconductors. *Phys. Rev. B* 57, 2454–2460 (1998).
16. Murray, C. B., Norris, D. J. & Bawendi, M. G. Synthesis and characterization of nearly monodisperse CdE (E = sulfur, selenium, tellurium) semiconductor nanocrystallites. *J. Am. Chem. Soc.* 115, 8706–8715 (1993).
17. Yu, D., Wang, C. & Guyot-Sionnest, P. n-Type conducting CdSe nanocrystal solids. *Science* 300, 1277–1280 (2003).
18. Wessels, J. M. *et al.* Optical and electrical properties of three-dimensional interlinked gold nanoparticle assemblies. *J. Am. Chem. Soc.* 126, 3349–3356 (2004).
19. Leatherdale, C. A. *et al.* Photoconductivity in CdSe quantum dot solids. *Phys. Rev. B* 62, 2669–2680 (2000).
20. Jarosz, M. V., Porter, V. J., Fisher, B. R., Kastner, M. A. & Bawendi, M. G. Photoconductivity of treated CdSe quantum dot films exhibiting increased exciton ionization efficiency. *Phys. Rev. B* 70, 195327 (2004).

21. Oertel, D. C., Bawendi, M. G., Arango, A. C. & Bulovic, V. Photodetectors based on treated CdSe quantum-dot films. *Appl. Phys. Lett.* **87**, 213505 (2005).

22. Hines, M. A. & Scholes, G. D. Colloidal PbS nanocrystals with size-tunable near-infrared emission: observation of post-synthesis self-narrowing of the particle size distribution. *Adv. Mater.* **15**, 1844–1849 (2003).

23. Yu, D., Wang, C., Wehrenberg, B. L. & Guyot-Sionnest, P. Variable range hopping mechanism in semiconductor nanocrystal solids. *Phys. Rev. Lett.* **92**, 216802 (2004).

24. Rahada, R. H. & Minden, H. T. Photosensitization of PbS films. *Phys. Rev.* **102**, 1258–1262 (1956).

25. Scher, H. Anomalous transit-time dispersion in amorphous solids. *Phys. Rev. B* **12**, 2455–2477 (1975).